Syntectonic sedimentation effects on the growth of fold-and-thrust belts

Charlotte Fillon, Ritske Huismans, Pieter van Der Beek

Publisher: GSA
Journal: GEOL: Geology
Article ID: G33531

Syntectonic sedimentation effects on the growth of fold-and-thrust belts

Charlotte Fillon[1, 2], Ritske S. Huismans[2], and Peter van der Beek[1]

[1]*Institut des Sciences de la Terre, Université Joseph Fourier, BP53, 38041 Grenoble, France*

[2]*Department of Earth Science, Bergen University, Bergen N-5007, Norway*

ABSTRACT

We use two-dimensional mechanical models to investigate the effects of syntectonic sedimentation on fold-and-thrust belt development, testing variable syntectonic (wedge-top and foredeep) sediment thicknesses and flexural rigidities. Model results indicate a first-order control of syntectonic sedimentation on thrust-sheet length and thrust spacing. Thrust sheets are longer when syntectonic sediment thickness and/or flexural rigidity increase. Comparison with observations from several fold-and-thrust belts confirms this first-order control of syntectonic sedimentation.

INTRODUCTION

The potential controls of surface processes on the tectonic evolution of mountain belts are slowly becoming better understood (e.g., Whipple, 2009). Whereas erosion can strongly influence the growth of orogenic hinterland regions (Beaumont et al., 1992; Willett, 1999), syntectonic sedimentation appears as a dominant control on external fold-and-thrust belt development (Bonnet et al., 2007; Boyer, 1995; Huiqi et al., 1992; Malavieille, 2010; Marshak and Wilkerson, 1992; Mugnier et al., 1997; Simpson, 2006; Stockmal et al., 2007; Storti and McClay, 1995). Erosion products from the core of a mountain belt are transported to the foreland and deposited while the orogenic wedge continues to grow, thus interacting with the development of the fold-and-thrust belt.

This interaction can be understood in terms of critical taper theory (Dahlen, 1984; Dahlen, 1990; Davis et al., 1983): sedimentation on top of the wedge increases the taper angle necessary to reactivate and create new internal thrusts, thus promoting wedge propagation on the décollement level; sedimentation on the lower part of the wedge having the opposite effect.

The influence of erosion and sedimentation on the structural development of fold-and-thrust belts has been studied principally using analogue models. Storti and McClay (1995), for instance, show that adding syntectonic sediments on top of a wedge reduces the number of thrusts, the internal shortening and the taper angle required for the wedge to be critical, leading to longer thrust sheets. The surface slope and geometry of fold-and-thrust belts are also affected by flexural controls on plate bending, which are not easily incorporated in analogue models (but see Hoth et al., 2007). Numerical models of fold-and-thrust belt development more easily integrate these effects and have now reached sufficiently high numerical resolution that their predictions can be compared with observations in natural systems (Stockmal et al., 2007). Here we use two-dimensional mechanical models to investigate depositional controls on fold-and-thrust belt development. Focusing in particular on the effects of syntectonic wedge-top and foredeep sedimentation and the influence of flexure, we show that both exert first-order controls on wedge geometry and thrust propagation: increasing the thickness of syntectonic sediments and/or flexural rigidity leads to the activation of fewer and longer thrust sheets.

We show that these general results are consistent with observational constraints on structure and syntectonic sedimentation in natural fold-and-thrust belts.

MODEL SET UP

We use a two-dimensional (2-D) Arbitrary Lagrangian-Eulerian (ALE) finite-element technique (Fullsack, 1995) to model thin-skinned fold-and-thrust belt development. The model consists of strain-weakening frictional-plastic materials that allow for localization of deformation (Stockmal et al., 2007; Huismans and Beaumont, 2003; see GSA Data Repository[1] for details).

The reference model (Fig. 1) consists of four materials: (I) a strong strain-weakening frictional-plastic material, representing basement rocks; (II) an intermediate-strength strain-weakening frictional-plastic material representing sedimentary rocks; (III) a very weak frictional-plastic internal décollement layer between these two, representing evaporites; and (IV) a second weak frictional-plastic décollement layer located at the base of the model. The initial geometry resembles a pre-existing wedge and an adjacent sedimentary basin. A 1 cm yr^{-1} velocity boundary condition is imposed on the right side and the base of the model (Fig. 1). The left side of the model domain is fixed horizontally, except at the base, where the basal décollement layer is evacuated at the same velocity. Gravitational loading is compensated by flexural isostasy.

Here we focus exclusively on the effects of sedimentation and do not include erosional processes. Syntectonic sedimentation starts at 5 m.y. in models 2–6. From that moment, all topography below a fixed reference height, representing base level, is filled with sediments (Fig. 1). This representation of sedimentation is very simple but is consistent with the first-order infilling geometry of an orogenic wedge and its foreland basin system (e.g., DeCelles and Giles, 1996): the accommodation space is filled by sediments that are subsequently deformed, and the elevation of the reference level forces sedimentation to occur only in the foredeep and wedge-top domains. Varying base level allows for testing the effect of varying sediment input to the foreland.

MODEL RESULTS

We present two sets of models that demonstrate the sensitivity to syntectonic sedimentation (Fig. 2) and to flexural rigidity (Fig. 3). The first set includes three models with no (Model 1), moderate (Model 2), and strong (Model 3) syntectonic sedimentation. The second set investigates the response to changes in flexural rigidity (from 10^{21} to 10^{23} N m) for moderate sedimentation.

Reference Model, No Deposition—Model 1

During the first 5 m.y., deformation only affects the strong “basement”, building an initial high-relief orogenic wedge with a system of pro- and retro-thrusts (Fig. 2a), a common feature of all models presented. After 5 m.y., deformation propagates to the intermediate-strength “pre-tectonic sedimentary rocks”, that deform contemporaneously with the hinterland wedge. From this time on, short thrusts develop in-sequence. All thrusts verge toward the foreland with a regular spacing of ~17 km. No back-thrusts develop and there is almost no reactivation or out-of-sequence thrusting. By 12 m.y., nine uniform-length thrust sheets have formed.

Moderate Deposition—Model 2

Model 2 includes syntectonic sedimentation up to an intermediate reference level after 5 m.y. (Fig. 2b). At 5 m.y., the pre-tectonic sedimentary rocks are back-thrusted while a basement duplex develops in the hinterland; syntectonic sedimentation occurs mainly in the foredeep area. The first frontal thrust initiates at 7 m.y., creating a 34-km-wide wedge-top basin. With further shortening, deformation migrates back into the internal parts of the wedge and is partitioned between frontal and basal accretion. At 9 m.y., flexural subsidence resulting from the growing internal wedge, provides more sediment accommodation space and the formation of a second smaller wedge-top basin between the two frontal thrusts. At 12 m.y., deformation is partitioned between the frontal thrust, the reactivated back-thrust, and internal basement deformation. The average thrust-sheet length is 30 km and the maximum sediment thickness is 4 km.

Strong Deposition—Model 3

The generic behavior of Model 3 is similar to Model 2 but the increased sediment thickness results in longer thrust sheets (Fig. 2c). The first external thrust emerges around 9 m.y., at ~100 km from the backstop, resulting in a 75-km-wide wedge-top basin. The frontal thrust breaks through the sediments, where they start forming a constant thickness foreland basin fill. At 9 m.y., shortening is still accommodated by the frontal thrust, which accumulates more displacement than in model 2. A second thrust initiates just before 12 m.y. The average thrust-sheet length is 70 km with a maximum sediment thickness of 9 km.

Sensitivity to Flexural Rigidity—Models 4–6

Models 4–6 test the sensitivity to variations in flexural rigidity for a constant intermediate base level, and are all shown at 8 m.y. (Fig. 3). Model 5, which has the reference model rigidity (10^{22} Nm), is very similar to Model 2. A lower flexural rigidity (Model 4; 10^{21} Nm) favors a narrow foreland basin and the formation of a shorter (34-

km-long) thrust sheet. In contrast, a higher flexural rigidity (Model 6; 10^{23} Nm) favors the development of a wide foreland basin and the formation of a 94-km-long thrust sheet.

DISCUSSION

The first-order evolution of all models is similar, independent of the amount of syntectonic sediments (Fig. 2): (1) initiation of a frontal thrust; (2) out-of-sequence internal deformation and passive retreat of the external thrust belt; (3) initiation of a new in-sequence thrust, reproducing a frontal accretion cycle (e.g., Hoth et al., 2007; DeCelles and Mitra, 1995). The main differences between the models are the locus and the timing of thrust activation.

The model without syn-orogenic sedimentation propagates most rapidly. Thrusts are very short, numerous, and do not accommodate much shortening, whereas the thrust-sheet length increases with the amount and extent of syntectonic sedimentation.

The first external thrust and the subsequent frontal thrusts emerge either at the point where the sediments taper out (Model 2) or where they start forming a constant-thickness foreland-basin fill (Model 3). The location of thrust initiation corresponds to the point where the total work needed to slide on the décollement and to break through the sediments is minimal (Hardy et al., 1998). When sediment deposits extend further (Model 3), the location of frontal thrust activation migrates toward the foreland. The extent and thickness of syntectonic sediments thus assert a first-order control on the location of the frontal thrusts.

The models presented here demonstrate that the extent and thickness of syntectonic sediments strongly affect the structural style of fold-and-thrust belts. The sediments are deposited horizontally, effectively stabilizing the wedge (e.g., Willett and

Schlunegger, 2010). In the most external parts, where the sediments are thinnest and the angle of the basal décollement (β) tends to zero, the wedge reaches a critical state. After the formation of the first thrust the surface slope α strongly decreases, stabilizing the wedge. Further syntectonic sedimentation in front of the active thrust enlarges the stable wedge and promotes formation of a new frontal thrust. Therefore, the overall development of the wedge follows critical-taper theory. However the localization and timing of thrust activation is strongly influenced by strain weakening and the evolution of the shear zones, which cannot be readily explained by the theory, as observed in other recent studies (Buiter, 2012; Simpson, 2011).

Flexure plays an important role in determining the structural style of a fold-and-thrust belt. The extent of sediment deposition is itself primarily governed by flexural parameters controlling the foreland basin shape. For lower flexural rigidities (Fig. 3, Model 4) a narrow and deep foreland basin is formed, limiting the extent of sedimentation with consequently shorter thrust sheets initiating where the sediments taper out. In contrast, for higher flexural rigidities a wider foreland basin develops, promoting sedimentation much further out in the foreland and formation of longer thrust sheets.

The location of the frontal thrust is also affected by the strength of the décollement level. A stronger décollement renders frontal accretion more difficult (see supplementary models in the Data Repository), but the reduction in thrust sheet length is moderate (a few kilometers) compared to the effect of syntectonic sedimentation. Therefore, the role of décollement strength appears of secondary importance in controlling the geometry of fold-and-thrust belts.

COMPARISON TO NATURAL SYSTEMS

The numerical models presented here demonstrate that syntectonic sedimentation exerts a major control on fold-and-thrust belt development. We compare our results to observed structural style, syntectonic sediment thickness, and flexural rigidity of several thin-skinned fold-and-thrust belts around the world (Fig. 4). Cross sections for three different fold-and-thrust belts (Pyrenees, Apennines, and Canadian Rockies) qualitatively illustrate the correlation between thrust-sheet length and syntectonic sediment thickness (Fig. 4a). The southern Pyrenean fold-and-thrust belt is characterized by a thick succession of syntectonic sediments, long thrust sheets and a wide wedge-top basin, transported over an efficient décollement level, comparable to 3 (Fig. 2c). The Apennines, with intermediate syntectonic sediment thickness, are characterized by moderate thrust-sheet length. The Canadian Rocky Mountains, where syntectonic sediments are thin or even absent, developed very short thrust sheets comparable to Model 1 (Fig. 2a).

The average thrust-sheet length of 8 fold-and-thrust belts is plotted as a function of maximum syntectonic sediment thickness in Figure 4b and according to the equivalent elastic thickness of the underlying lithosphere. Although these fold-and-thrust belts differ strongly in age and tectonic setting, a clear correlation between the thickness and extent of syntectonic sedimentation and thrust-sheet length appears. The effect of flexural rigidity is less obvious, although ranges developed on thicker elastic lithosphere appear to be characterized by the longest thrust sheets. Only the Brooks Range (Alaska) lies outside the observed trend. However, low-temperature thermochronology indicates that post-orogenic erosion has removed several kilometers of sediment from this range (O'Sullivan et al., 1997), so that syntectonic deposits may have been much thicker initially. Including these sediments aligns this system with the observed trend.

CONCLUSIONS

We have presented mechanical models that provide a general explanation for the effects of syntectonic sedimentation on the formation of thin-skinned fold-and-thrust belts. The model results show that an increase in syntectonic sedimentation leads to significantly longer thrust sheets. Increases in flexural rigidity enhance this effect by widening the basin and therefore extending the area of sediment deposition. A range of natural thin-skinned fold-and-thrust belts shows a linear correlation between maximum sediment thickness and thrust-sheet length, confirming the inference from the numerical models.

ACKNOWLEDGMENTS

This study is supported by Institut national des sciences de l'Univers - CNRS through the European Science Foundation Topo-Europe project "Spatial and temporal coupling between tectonics and surface processes during lithosphere inversion of the Pyrenean-Cantabrian Mountain belt (PyrTec)". We thank Sean Willett for constructive comments on an earlier version of this work. Peter DeCelles and Jacques Malavieille are thanked for insightful reviews that helped improving the manuscript.

REFERENCES CITED

Beaumont, C., Fullsack, P., and Hamilton, J., 1992, Erosional control of active compressional orogens, *in* McClay, K.R., ed., Thrust Tectonics: London, Chapman & Hall, p. 1–18.

Bonnet, C., Malavieille, J., and Mosar, J., 2007, Interactions between tectonics, erosion, and sedimentation during the recent evolution of the Alpine orogen: Analogue modeling insights: Tectonics, v. 26, TC6016, doi:10.1029/2006TC002048.

Boyer, S.E., 1995, Sedimentary basin taper as a factor controlling the geometry and advance of thrust belts: American Journal of Science, v. 295, p. 1220–1254, doi:10.2475/ajs.295.10.1220.

Buiter, S.J.H., 2012, A review of brittle compressional wedge models: Tectonophysics, v. 530–531, p. 1–17, doi:10.1016/j.tecto.2011.12.018.

Dahlen, F.A., 1984, Noncohesive Critical Coulomb Wedges: An Exact Solution: Journal of Geophysical Research, v. 89, p. 10125–10133, doi:10.1029/JB089iB12p10125.

Dahlen, F.A., 1990, Critical taper model of fold-and-thrust belts and accretionary wedges: Annual Review of Earth and Planetary Sciences, v. 18, p. 55–99, doi:10.1146/annurev.ea.18.050190.000415.

Davis, D., Suppe, J., and Dahlen, F.A., 1983, Mechanics of fold-and-thrust belts and accretionary wedges: Journal of Geophysical Research, v. 88, p. 1153–1172, doi:10.1029/JB088iB02p01153.

DeCelles, P., and Giles, K.A., 1996, Foreland basin systems: Basin Research, v. 8, p. 105–123, doi:10.1046/j.1365-2117.1996.01491.x.

DeCelles, P.G., and Mitra, G., 1995, History of the Sevier orogenic wedge in terms of critical taper models, northeast Utah and southwest Wyoming: Geological Society of America Bulletin, v. 107, p. 454–462, doi:10.1130/0016-7606(1995)107<0454:HOTSOW>2.3.CO;2.

Fullsack, P., 1995, An arbitrary Lagrangian-Eulerian formulation for creeping flows and its application in tectonic models: Geophysical Journal International, v. 120, p. 1–23, doi:10.1111/j.1365-246X.1995.tb05908.x.

Hardy, S., Duncan, C., Masek, J., and Brown, D., 1998, Minimum work, fault activity and the growth of critical wedges in fold and thrust belts: Basin Research, v. 10, p. 365–373, doi:10.1046/j.1365-2117.1998.00073.x.

Hoth, S., Hoffmann-Rothe, A., and Kukowski, N., 2007, Frontal accretion: An internal clock for bivergent wedge deformation and surface uplift: Journal of Geophysical Research, v. 112, p. B06408.B06408, doi:10.1029/2006JB004357

Huiqi, L., McClay, K.R., and Powell, D., 1992, Physical models of thrust wedges, *in* McClay, K.R., ed., Thrust tectonics: London, Chapman & Hall, p. 71–81.

Huismans, R.S., and Beaumont, C., 2003, Symmetric and asymmetric lithospheric extension: Relative effects of frictional-plastic and viscous strain softening: Journal of Geophysical Research, v. 108, p. 2496, doi:10.1029/2002JB002026.

Malavieille, J., 2010, Impact of erosion, sedimentation, and structural heritage on the structure and kinematics of orogenic wedges: Analog models and case studies: GSA Today, v. 20, p. 4–10, doi:10.1130/GSATG48A.1.

Marshak, S., and Wilkerson, M.S., 1992, Effect of overburden thickness on thrust belt geometry and development: Tectonics, v. 11, p. 560–566, doi:10.1029/92TC00175.

Mugnier, J.L., Baby, P., Colletta, B., Vinour, P., Bale, P., and Leturmy, P., 1997, Thrust geometry controlled by erosion and sedimentation: A view from analogue models: Geology, v. 25, p. 427–430, doi:10.1130/0091-7613(1997)025<0427:TGCBEA>2.3.CO;2.

Muñoz, J.A., 1992, Evolution of a continental collision belt: ECORS Pyrenees crustal balanced cross section, *in* McClay, K.R., ed., Thrust Tectonics: London, Chapman & Hall, p. 235–246.

O'Sullivan, P.B., Murphy, J.M., and Blythe, A.E., 1997, Late Mesozoic and Cenozoic thermotectonic evolution of the central Brooks Range and adjacent North Slope foreland basin, Alaska: Including fission track results from the Trans-Alaska Crustal Transect (TACT): Journal of Geophysical Research, v. 102, p. 20821–20845, doi:10.1029/96JB03411.

Ollerenshaw, N.C., 1978, Calgary, Alberta–British Columbia: Canada, Geological Survey of Canada, Map 1457A, scale 1:250000, 2 sheets.

Pieri, M., 1989, Three seismic profiles through the Po Plain, *in* Bally, A.W., ed., Atlas of Seismic Stratigraphy, Volume 27/3: Tulsa, Oklahoma, American Association of Petroleum Geologists, p. 90–110.

Simpson, G., 2011, Mechanics of non-critical fold-and-thrust belts based on finite element models: Tectonophysics, v. 499, p. 142–155, doi:10.1016/j.tecto.2011.01.004.

Simpson, G.D.H., 2006, Modelling interactions between fold-and-thrust belt deformation, foreland flexure and surface mass transport: Basin Research, v. 18, p. 125–143, doi:10.1111/j.1365-2117.2006.00287.x.

Stockmal, G.S., Beaumont, C., Nguyen, M., and Lee, B., 2007, Mechanics of thin-skinned fold-and-thrust belts: Insights from numerical models, *in* Sears, J.W., Harms, T.A., and Evenchick, C.A., eds., Whence the Mountains? Inquiries into the Evolution of Orogenic Systems: A Volume in Honor of Raymond A. Price, Volume

433: Geological Society of America Special Paper 433, p. 63–98.10.1130/2007.2433(04)

Storti, F., and McClay, K., 1995, Influence of syntectonic sedimentation on thrust wedges in analogue models: Geology, v. 23, p. 999–1002, doi:10.1130/0091-7613(1995)023<0999:IOSSOT>2.3.CO;2.

Whipple, K.X, 2009, The influence of climate on the tectonic evolution of mountain belts: Nature Geoscience, v. 2, p. 97–104, doi:10.1038/ngeo413.

Willett, S.D., 1999, Orogeny and orography: The effects of erosion on the structure of mountain belts: Journal of Geophysical Research, v. 104, p. 28957–28981, doi:10.1029/1999JB900248.

Willett, S.D., and Schlunegger, F., 2010, The last phase of deposition in the Swiss Molasse Basin: From foredeep to negative-alpha basin: Basin Research, v. 22, p. 623–639, doi:10.1111/j.1365-2117.2009.00435.x.

FIGURE CAPTIONS

Figure 1. Model geometry and boundary conditions. Dotted line on the right side of the box represents the continuity of the Lagrangian grid up to 800 km from the backstop; Eulerian grid extends to 400 km. Syntectonic deposition starts at 5 m.y. See text and Table DR1 (see footnote 1) for model parameter values.

Figure 2. Model evolution with different amounts of syntectonic sedimentation. A: Model 1: no syntectonic sedimentation. B: Model 2: syntectonic sedimentation up to 1.95 km elevation. C: Model 3: syntectonic sedimentation up to 3 km elevation. Panels show development at 5, 7, 9, and 12 m.y. Flexural rigidity is 10^{22} N m.

Figure 3. Sensitivity to flexural rigidity. Panels show evolution at 8 m.y. for Models 4–6 with varying flexural rigidity (Model 4: 10^{21} N m; Model 5: 10^{22} N m; Model 6: 10^{23} N m), corresponding to elastic thicknesses of 4.8, 10.4, and 22.4 km, respectively (for Poisson ratio of 0.25 and Young's modulus of 10^{11} N m^{-2}). Models were run with syntectonic sedimentation reference level of 2.15 km.

Figure 4. A: Simplified cross-sections of fold-and-thrust belts with different thicknesses of syntectonic sediments and thrust-sheet lengths; from top to bottom: Canadian Rockies (Ollerenshaw, 1978), northern Apennines (Pieri, 1989), and ECORS section, Pyrenees (Muñoz, 1992). B: Average thrust-sheet length plotted against maximum sediment thickness for the Western Alps, France (Alp); Sub-Andean belt, North-West Bolivia (An1) and South Bolivia (An2); Northern Apennines (Ap); Brooks Ranges, Alaska (Br); Canadian Rockies (Can); Carpathians (Car) and Southern Pyrenees (Pyr). The maximum sediment thickness and thrust-sheet length were measured on at least three thrust sheets of the fold-and-thrust belt and then averaged; see Table DR2 (see footnote 1) for values and references.

[1]GSA Data Repository item 2012xxx, xxxxxxxx, is available online at www.geosociety.org/pubs/ft2012.htm, or on request from editing@geosociety.org or Documents Secretary, GSA, P.O. Box 9140, Boulder, CO 80301, USA.

Figure 1
Click here to download Figure: fig1NB.pdf

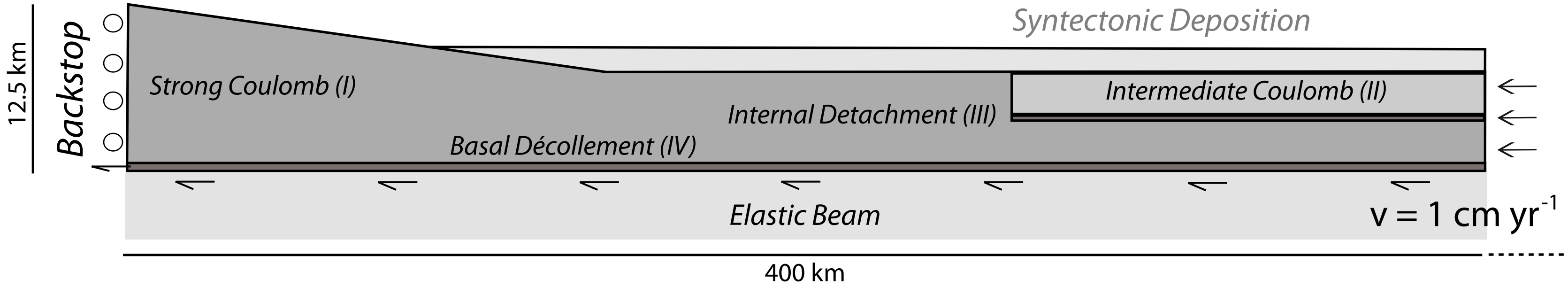

Figure 2
Click here to download Figure: fig2_resized.pdf

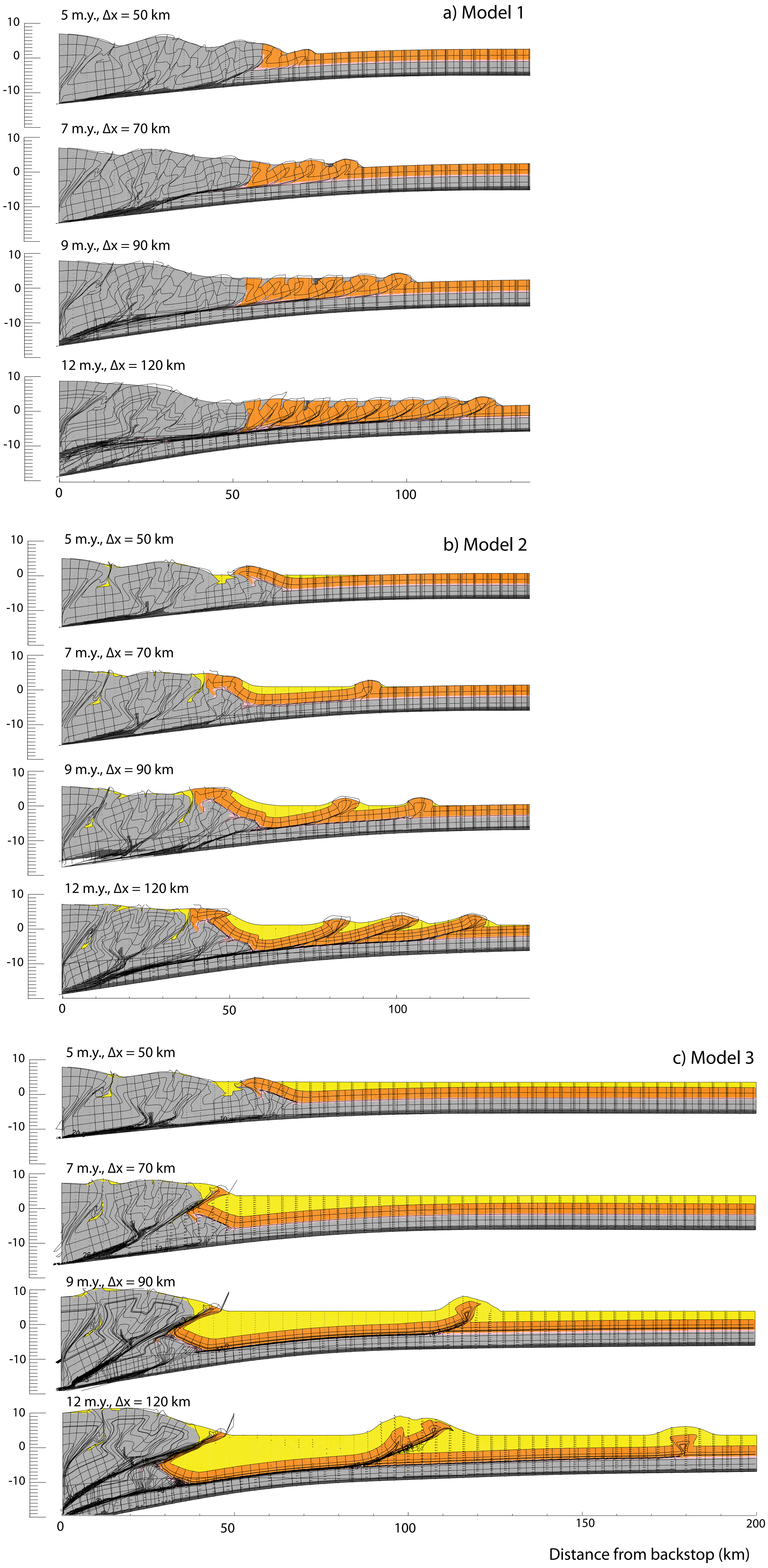

Figure 3

Click here to download Figure: fig3.pdf

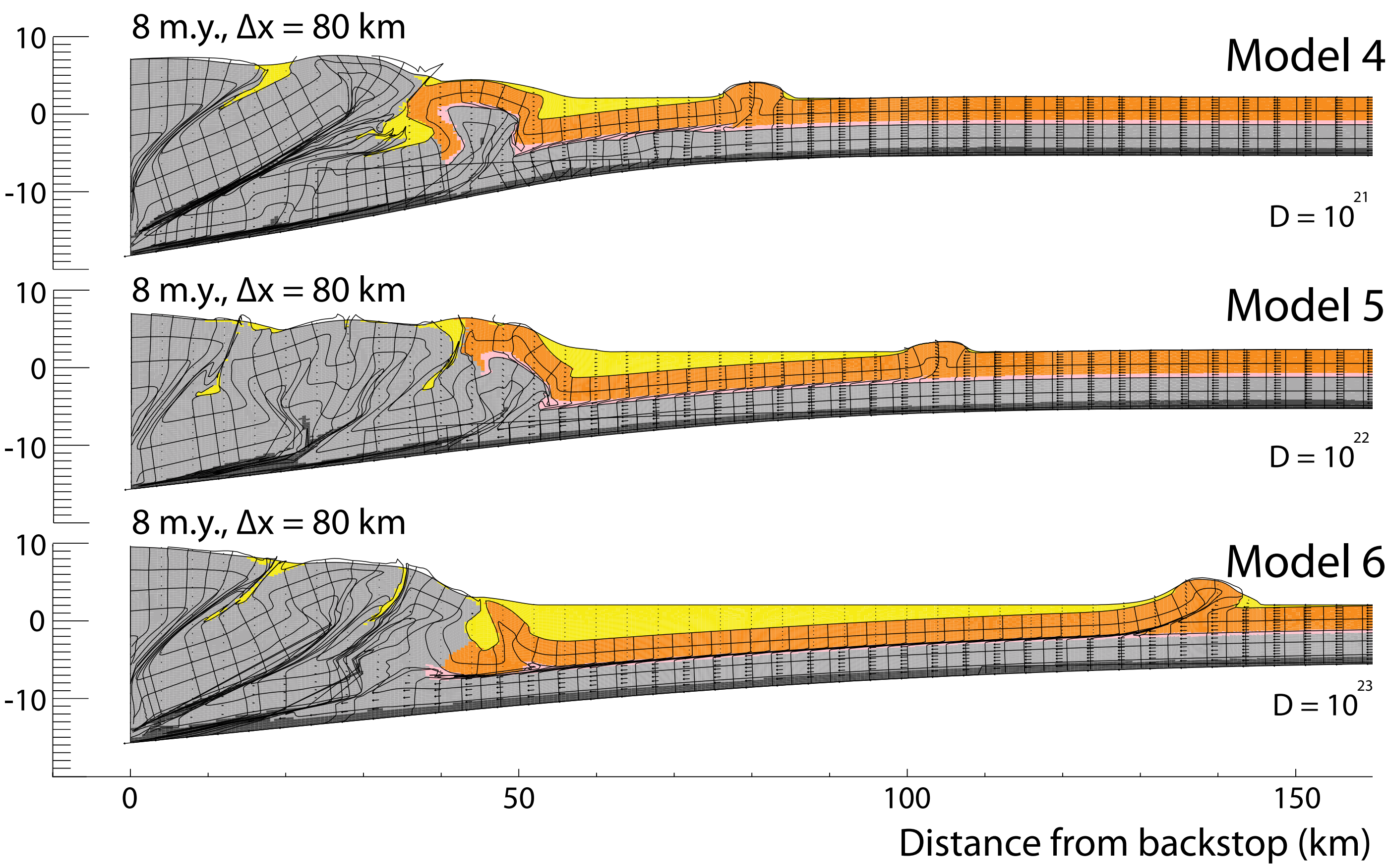

Figure 4

Click here to download Figure: Fig4.pdf

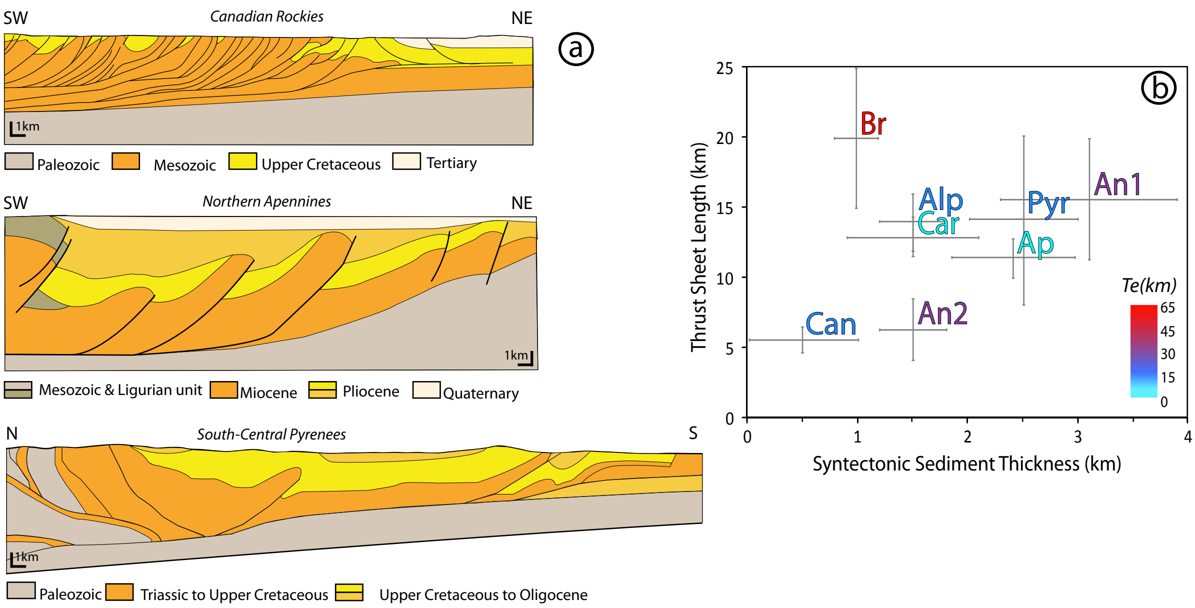

Movie File
Click here to download Movie File: model2.mov

SUPPLEMENTARY MATERIAL

Supplementary methods

Rheology

In order to reproduce and localize deformation in frictional-plastic shear zones, the model uses a plastic yield criterion. Once yielding occurs, materials of the deformed area experience strain softening. In this model, the Drucker-Prager pressure-dependent yield criterion is used to model the plastic behavior for incompressible deformation in plane strain. Yielding occurs when:

$$(J_2)^{\frac{1}{2}} = p \sin\phi(\varepsilon) + c\cos\phi(\varepsilon). \qquad (1)$$

Where $J_2 = \frac{1}{2}\sigma_{ij}\sigma_{ij}$ is the second invariant of the deviatoric stress, p is the dynamic pressure (mean stress), c is the cohesion and ϕ is the internal friction angle. The values of c and $\phi(\varepsilon)$ were chosen to reproduce frictional sliding of rocks. Several mechanisms can lead to brittle weakening of rocks (Huismans and Beaumont, 2007 and references therein), including cohesion loss, mineral transformations, and increased pore fluid pressures. In the models presented here strain weakening is introduced using a parametric approach. The friction angle $\phi(\varepsilon)$ decreases linearly with increasing strain in the range $0.5< \varepsilon <1.0$, where ε represents the square root of the second invariant of deviatoric strain.

Model set up

The initial model has a computational Eulerian domain 400 km long, 12.5 km high on the left-hand side and 7.5 km high on the right-hand side. The Lagrangian material-tracking grid follows the initial Eulerian domain but extends until 800 km (e.g. Supplementary Table 1). Materials II and III (representing the sediments and the internal décollement respectively) extend from 100 km to the right-hand side of the model, in order to allow for a first stage of deformation in the internal wedge to occur close to the backstop. Material II is 3 km thick, and Material III is 0.5 km thick, so that Materials II and III have the same thickness on the right-hand side of the model, and the décollement level is located in the middle of the model area. A second décollement level has been added to the base of the model, which is 1 km thick. A velocity of -1 cm.yr^{-1} is applied to the right-hand boundary, while the left-hand side is fixed horizontally, except in the first km, to evacuate the basal décollement layer with a velocity of 1 cm.yr^{-1}. The surface is subjected to sedimentation after 5 m.y, represented by the deposition of material with the same properties as Material II below a fixed reference elevation; erosion has not been included in our models. The base of the model is supported by an elastic beam that allows for flexural isostasy.

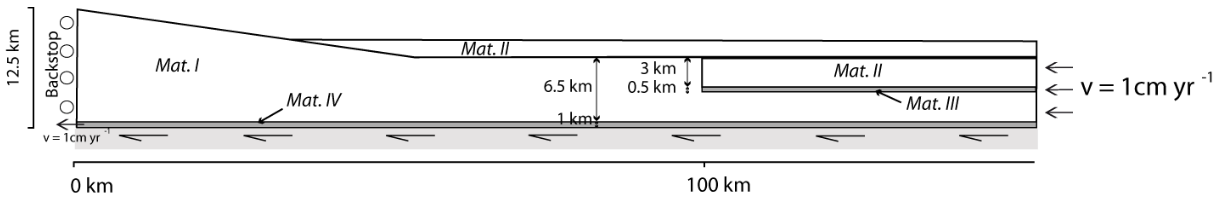

Supplementary Figure S1: *Initial model geometry.*

Models parameters values

Material number	Description	Internal friction angle Φ	
		Φ1	**Φ2**
I	Strong Coulomb, with strain softening	38	25
II	Intermediate Coulomb, with strain softening	38	18
III	Very weak internal décollement	1	
IV	Weak basal décollement	10	
Cohesion	2 MPa		
Density	2300 $km.m^{-3}$		
Eulerian grid	801 x 81 cells	400 x 12.5 km	
Lagrangian grid	1601 x 81 cells	800 x 12.5 km	

Supplementary Table 1*: Fixed parameter values for numerical model runs.*

Supplementary models

Influence of the strength of internal décollement on the thrust sheet lengths

The rheology of the internal décollement can form a major control on the wedge development. In order to test this influence, we have run several models with increasing the strength of the internal décollement material (characterized by its internal friction angle ϕ). We present in supplementary Figure S2 snapshots of models with ϕ at 2°, 4°, 6°, and 8° at the time when the first external thrust activates. Syn-tectonic sedimentation in these supplementary models starts at 3 m.y. and was set at the same level as in the model 2 (Figure 2) for models in panels a to d, and at a higher reference level, covering entirely the basin for models in panels e to h.

Models a-d demonstrate that despite differences in structural styles (in particular in models c and d), the sedimentary thrust sheets formed have a shorter length with increasing décollement strength, ϕ. The first thrust activates at 95, 97, 92 and 84 km from the backstop, in model a, b, c, and d respectively. Models e-h show a similar response to increasing the décollement strength with the higher reference level for sedimentation. The thrusts are shorter for a stronger décollement level, and activate at 112, 107, 86 and 88 km in models e, f, g and h respectively. We note that in models g and h (ϕ = 6° and 8°), the basement and the sedimentary layers deform jointly, because the difference in strength between the basement, the décollement and the sedimentary layer is small.

We thus conclude from this set of models that the rheology of the décollement level has an impact on the thrust sheet length by shortening them, but this effect is much less significant than the effect of syn-tectonic wedge-top sedimentation on the wedge propagation and thrust sheet length. Moreover, the models confirm that also with a large amount of syn-tectonic deposition covering both the wedge and the fore-deep the thrust sheets are very long.

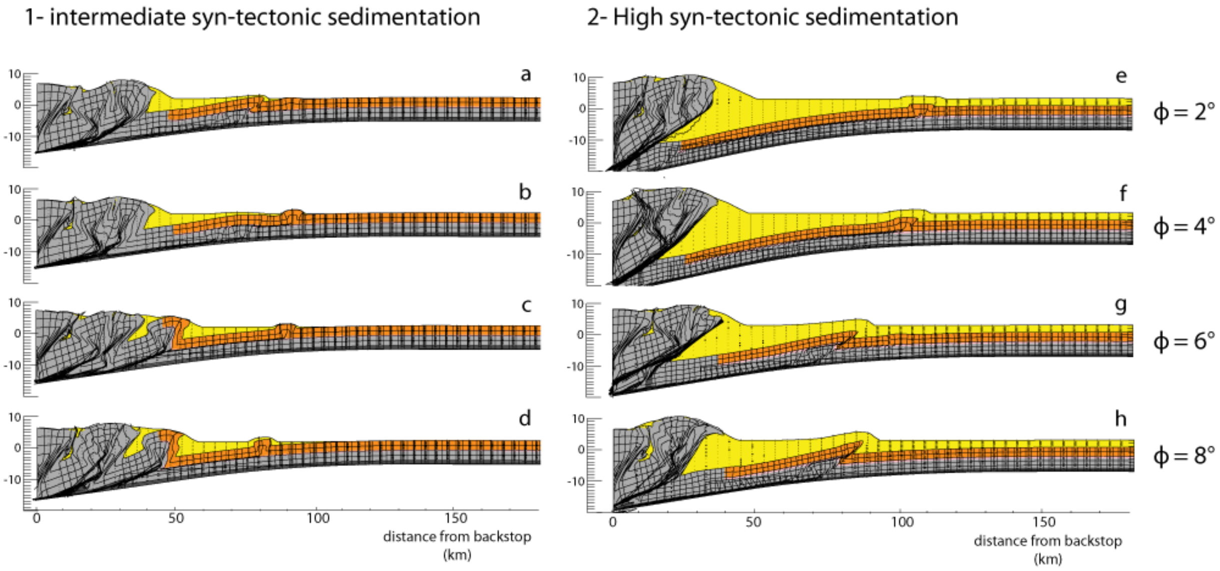

Supplementary Figure S2: *Tests of the influence of the strength of the internal decollement on thrust sheet length. For models a to d, model set up is the same as in model 2 (Figure 2) but with syn-tectonic sedimentation starting at 3 Ma. For models e to h, the reference elevation for the syn-tectonic sedimentation was set to 3 km, resulting in sediments covering the complete foreland basin. The strength of the décollement is represented by the internal friction angle ϕ, that is 2°, 4°, 6°, and 8° for models a and e, b and f ,c and g , d and h respectively. Models snapshots are shown at the time when the first external thrust activates.*

Strain rates and velocity field

Supplementary Figure S3 documents the strain-rate evolution for the same models and at the same timesteps as shown in Figure 2. The green zones (at 7 m.y. in models 1 and 3 for example) show the diffuse pattern of strain partitioning that is subsequently followed by localization on large faults. In the three models, most of the material advection from the right side of the model is accommodated by the fontal thrust and by underthrusting below the décollement level. In Model 1 (without syn-tectonic sedimentation), at 5 my, displacement is localized at the front but in the internal parts as well, with active backthrusting at around 50 km. Then this internal displacement progressively decreases to almost zero at 12 m.y. The velocity field in the fold-and-thrust belt shows that each thrust is active, but always less than the frontal thrust. Model 2 and 3 are very similar in terms of velocity field patterns. The backthrusting that occurs at 5 m.y. is very efficient at that time while the internal part experiences little displacement. Between 7 and 9 m.y. the frontal thrust records most of the displacement, and the internal part (especially around 50 km from the backstop) show moderate and upward-directed velocities. Finally, at 12 m.y., only the fold-and-thrust belt records displacement, and the internal part become much less active. It is also worth noting that the velocity field shows the progression of under-thusting below the internal decollement level towards the left side of the model. Strain localization allows identifying the most active faults. In the three models, the strain is accumulated on 1) the frontal thrust, 2) the décollement level, and 3) the largest shear zones in the internal parts, with the décollement level concentrating most strain.

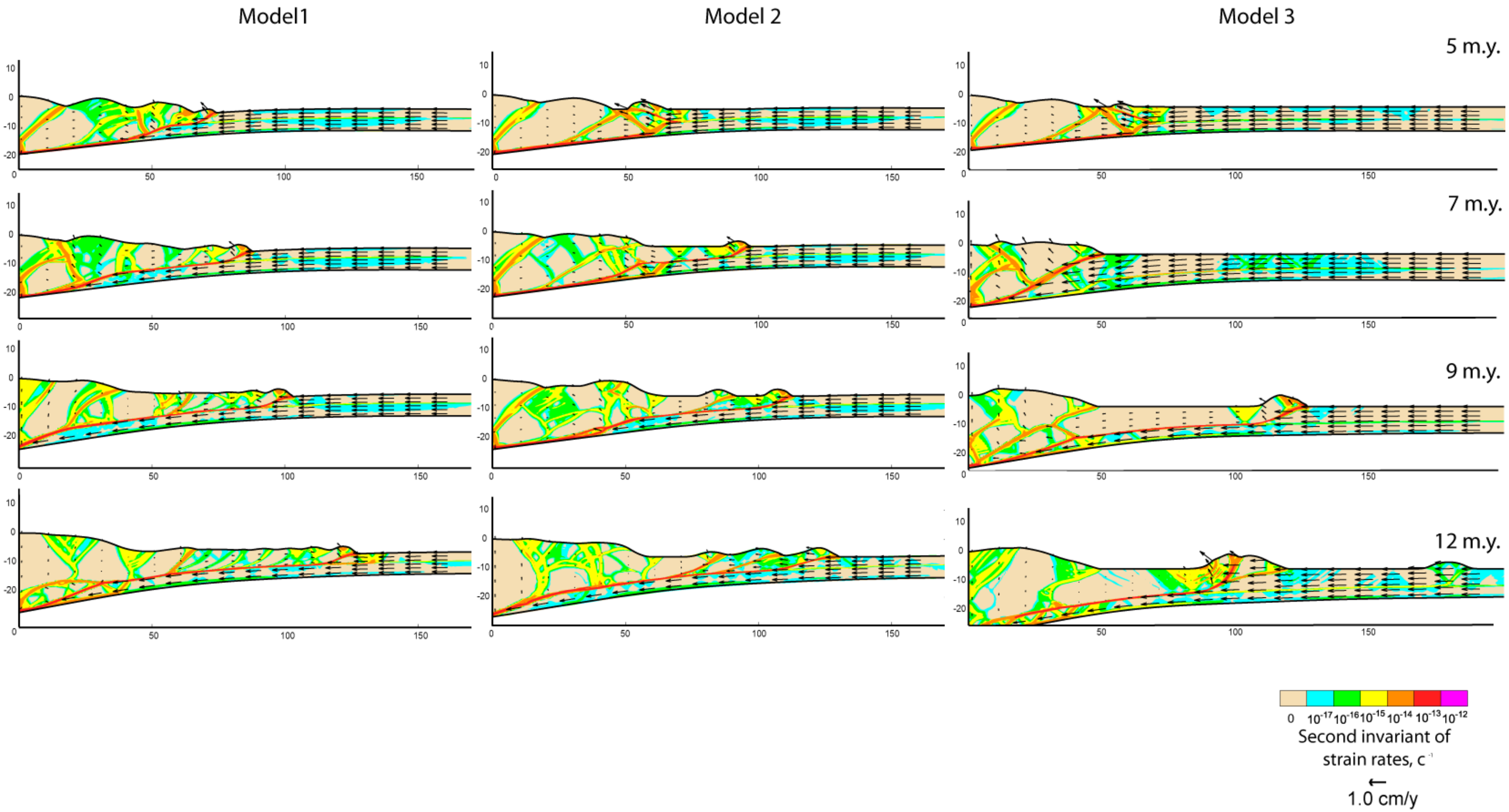

***Supplementary Figure S3**: Evolution of second invariant of deviatoric strain rate and velocity field for models/snapshots shown in Figure 2 (main paper).*

Data and references for natural systems

Range	Average thrust length (km)	Maximum thickness of syn-tectonic sediments (km)	Reference for cross-sections	Elastic thickness (km)	Reference for Te
Canadian Rockies (Can)	5.5 ± 3.1	1.5 ± 0.7	*Ollerenshaw, 1978*	20 to 40	*Flück et al., 2003*
Sub-andean belt (An2, S Bolivia)	6.3 ± 2.2	1.5 ± 0.3	*Horton, 1998*	30 to 40	*DeCelles and Horton, 2003a*
Apennines (Ap)	8.6 ± 4.1	1.8 ± 0.6	*Butler et al., 2004*	8 to 15	*Royden and Karner, 1984*
Carpathians (Car)	12.9 ± 1.4	1.5 ± 0.6	*Hippolyte et al., 1999*	3 to 16	*Zoetemeijer et al., 1999*
Pyrenees (Pyr)	13.8 ± 4.6	2.5 ± 0.3	*Muñoz, 1992*	20 to 30	*Zoetemeijer et al., 1990*
Swiss molassic basin (Alp)	14 ± 2	1.5 ± 0.3	*Beck et al., 1998*	5 to 15	*Sinclair et al., 1991*
Sub-andean belt (An1, NW Bolivia)	15.6 ± 4.3	3.1 ± 0.8	*Baby et al., 1995*	30 to 40	*DeCelles and Horton, 2003b*
Brooks ranges (Br)	20 ± 5	1 ± 0.2	*Cole et al., 1997*	65 to 75	*Nunn et al., 1987*

Supplementary Table 2*: Sediment thicknesses, thrust-sheet lengths, and equivalent elastic thicknesses for natural fold-and-thrust belts. Measurements of thrust sheet length and their associated syn-tectonic sedimentation thickness was taken in three places of the fold-and thrust belt at least .The sediment thickness was measured at the place where the vertical thickness is maximum, i.e in the center of a piggy-back basin for example. The thrust sheet length was defined by the length from the place where the thrust is differentiating to its surface emergence.*

References

Baby, P., Limachi, R., Moretti, I., Mendez, E., Oller, J., Guiller, B., and Specht, M., 1995, Petroleum system of the northern and central Bolivian sub-Andean zone, *in* A.J.Tankard, Suarez, R., and Welsink, H.J., eds., Petroleum Basins of South America, Volume American Association of Petroleum Geologists Memoir, 62, p. 445-458.

Beck, C., Deville, E., Blanc, E., Philippe, Y., and Tardy, M., 1998, Termination of the Savoy Molasse Basin (northwestern siliciclastic accumulation (Upper Marine Molasse) in the southern Alps/southern Jura), *in* Mascle, A., Puigdefàbregas, C., Luterbacher, H.P., and Fernàndez, M., eds., Cenozoic Foreland Basins of Western Europe, Volume Geological Society, London, Special Publication, 134, p. 263-278.

Butler, R.W.H., Mazzoli, S., Corrado, S., De Donatis, M., Di Bucci, D., Gambini, R., Naso, G., Nicolai, C., Scrocca, D., Shiner, P., and Zucconi, V., 2004, Applying thick-skinned tectonic models to the Apennine thrust belt of Italy—Limitations and implications, *in* McClay, K.R., ed., Thrust tectonics and hydrocarbon systems, Volume 82, p. 647– 667.

Cole, F., Bird, K.J., Toro, J., Roure, F., O'Sullivan, P.B., Pawlewicz, M., and Howell, D.G., 1997, An integrated model for the tectonic development of the frontal Brooks Range and Colville Basin 250 km west of the Trans-Alaska Crustal Transect: Journal of Geophysical Research, v. 102, p. 20685-20708.

DeCelles, P., and Horton, B.K., 2003a, Early to middle Tertiary foreland basin development and the history of Andean crustal shortening in Bolivia: GSA Bulletin, v. 115, p. 58-77.

—, 2003b, Early to middle Tertiary foreland basin development and the history of Andean crustal shortening in Bolivia: Geological Society of America Bulletin, v. 115, p. 58-77.

Flück, P., Hyndman, R.D., and Lowe, C., 2003, Effective elastic thickness T e of the lithosphere in western Canada: Journal of Geophysical Research, v. 108, p. 2430.

Hippolyte, J.C., Badescu, D., and Constantin, P., 1999, Evolution of the transport direction of the Carpathian belt during its collision with the east European Platform: Tectonics, v. 18, p. 1120-1138.

Horton, B.K., 1998, Sediment accumulation on top of the Andean orogenic wedge: Oligocene to late Miocene basins of the Eastern Cordillera, southern Bolivia: Geological Society of America Bulletin, v. 110, p. 1174-1192.

Huismans, R.S., and Beaumont, C., 2007, Roles of lithospheric strain softening and heterogeneity in determining the geometry of rifts and continental margins, *in* Karner, G.D., Manatschal, G., & Pinhiero, L.M. , ed., Imaging, Mapping and Modelling Continental Lithosphere Extension and Breakup, Geological Society, London, Special Publications, p. 107-134.

Muñoz, J.A., 1992, Evolution of a continental collision belt: ECORS Pyrenees crustal balanced cross section, *in* McClay, K.R., ed., Thrust Tectonics: London, Chapman & Hall, p. 235-246.

Nunn, J.A., Czerniak, M., and Pilger, R.H.J., 1987, Constraints on the structure of Brooks Range and Colville Basin, Northern Alaska, from flexure and gravity analysis.: Tectonics, v. 6, p. 603-617.

Ollerenshaw, N.C., 1978, Geology, Calgary, Alberta–British Columbia, Geological Survey of Canada Map 1457A.

Royden, L., and Karner, G.D., 1984, Flexure of Lithosphere Beneath Apennine and Carpathian Foredeep Basins: Evidence for an Insufficient Topographic Load: AAPG Bulletin, v. 68.

Sinclair, H.D., Coakley, B.J., Allen, P.A., and Watts, A.B., 1991, Simulation of Foreland Basin Stratigraphy using a diffusion model of mountain belt uplift and erosion: An example from the central Alps, Switzerland: Tectonics, v. 10, p. 599-620.

Zoetemeijer, R., Desegaulx, P., Cloetingh, S., Roure, F., and Moretti, I., 1990, Lithospheric Dynamics and Tectonic-startigraphic Evolution of the Ebro basin: Journal of Geophysical Research, v. 95, p. 2701-2711.

Zoetemeijer, R., Tomek, C., and Cloetingh, S., 1999, Flexural expression of European continental lithosphere under the western outer Carpathians: Tectonics, v. 18, p. 843-861.